Numerical Investigation of Void Fraction Distribution for Comparative Analysis of Flow Patterns Repartition in Thermal Driven Bubble Pumps

R. Garma[#1], D. Sioud[#2], Y. Stiriba[*3], M. Bourouis[*4], A. Bellagi[#5]

[#] *National Engineering School of Monastir, Unit of Thermic and Thermodynamics of the Industrial Processes, Ibn El Jazzar street, 5019 Monastir, Tunisia*

raoudhagarma83@gmail.com

[2]siouddoniazed@gmail.com

[5]a.bellagi@enim.rnu.tn

[*]*Department of Mechanical Engineering, Universitat Rovira i Virgili, Av. Països Catalans No. 26, 43007 Tarragona, Spain*

[3]youssef.stiriba@urv.cat

[4]mahmoud.bourouis@urv.cat

***Abstract*— Bubble pump, one of the most important component are in the diffusion absorption machine, is used for the circulation of the liquid mixture and has a considerable influence on its performances. In the present paper, numerical simulation of the heating repartition effect on the boiling flow in this component is performed with the commercial CFD package ANSYS-FLUENT 12.0. Eulerian multiphase flow framework is used to model the phases' interactions. User-Defined Functions (UDFs) are provided to compute the wall heat transfer and to calculate the inter-phase heat and mass transfer. Heat is supplied at the wall of the pump tube. Full and partial pipe heating are considered to exanimate two different configurations of the bubble pump. Pure water is used as working fluid. The void fraction distribution is calculated in order to localize the onset of vapor generation and to predict the flow patterns throughout the tube length.**

***Keywords*— Bubble pump configuration, Tube heating, Boiling flow, Void fraction, Flow patterns, CFD Simulation**

I. INTRODUCTION

Several advantageous characteristics such as the absence of mechanical moving part, causing vibration and noise, and specially the possibility to operate with waste heat or solar energy, attracted the attention of researchers to experimental and numerical investigations of diffusion absorption refrigerators (DARs) invented by Platen and Munters [1] in the 1920s. In these absorption systems, the bubble pump is an essential component. Therefore, significant attention has been devoted to this device to improve its performance, which would contribute to the performance of the whole system. The thermally driven bubble pump is a simple vertical tube which can be powered by heat from any source (electricity, burner, waste heat, solar energy). When the liquid solution is heated up, vapor bubbles are generated causing pressure difference between the bottom and the top of the tube. As result, natural circulation of the liquid solution is occurring through the tube and so boiling flow takes place inside the bubble pump. Zohar et al.[2] developed and analyzed by computer simulation a detailed thermodynamic model for three generator and bubble pump configurations of a DAR to study their effect on the system performance. A mathematical model for the forced convective boiling of refrigerant-absorbent mixtures in vertical tubular generator is proposed by Pasupathy et al. [3]. A parametric analysis has been performed to study the effect of various factors on the performance of the generator. Two-fluid model is employed by Ma et al. [4] to describe the two-phase flow and heat transfer processes in a two-phase closed thermosyphon. Numerically predicted flow patterns and distribution of parameters under different conditions show a good agreement with experimental results. Taieb et al. [5,6] tested the pumping capacity of bubble pumps by using Behringer correlation (cited in Ref. [7]). Uniformly heated bubble pump configuration was numerically investigated by Garma et al. [8,9] using the commercial CFD package ANSYS-FLUENT. It was found that the onset boiling point is reduced and the void fraction at tube's outlet is increased when the wall heat input is increased. An experimental investigation of an air-cooled diffusion-absorption machine operating with a binary light hydrocarbon mixture is presented by Ben Ezzine et al. [10]. A new concept of generator consisting in a separated boiler and bubble pump instead of the usual combined generator is tested. The experimental results show that the bubble pump exiting temperature as well as those of the major components of the machine is very sensitive to the heat input to the bubble pump. Experimental study and theoretical thermodynamic

ISSN: 2356-5608

simulations of the same absorption refrigerator prototype with methylamine-water-helium were carried out by Mazzouz et al. [11]. The test showed that all machine's components are very sensitive to the behaviour of the bubble pump. The performance of three different indirectly heated solar powered bubble pumps/generators were investigated and discussed by Jacob et al. [12,13,14,15].

Research effort has been also focused on predicting the flow regime transition using the void fraction profile. Radovich and Moissis [16] considered that the bubbly to slug flow transition is due to the collisions between small bubbles and supposed the transition to occur when the maximum packing of these small bubbles is reached. They suggested that this is the case when the void fraction is around 0.3. This same value was proposed by Taitel et al. [17] and Mishima et al. [18]. On the other side, Brauner et al. [19] and Barnea [20] claimed that the slug to churn transition takes place when the gas void fraction in the liquid slug reaches 0.52 corresponding to the maximum cubic lattice packing fraction. Transition from intermittent (slug or churn) flow to annular flow pattern can be observed when the vapor flow rate becomes sufficiently high. Wallis [21] suggested a transition void fraction of 0.8 after comparing void fraction data with theoretical prediction for intermitting and annular flow.

In the present paper, a CFD analysis of a bubble pump using the commercial package ANSYS-FLUENT is worked out. Full and partial length heating tube are considered in order to compare both configurations of thermally driven pump. Void fraction profiles for different heat fluxes are predicted and the evolution of flow patterns throughout the tube length is discussed.

II. MODEL DESCRIPTION

Mathematical model utilized in this paper was developed and then applied in CFD codes to be finally implemented in ANSYS-FLUENT via user-defined functions (UDFs) in conjunction with the Eulerian multiphase model in which the conservation equations are written for each phase, liquid and vapor.

The following is a summary of the main model equations for a certain phase q.

A. Conservation equations

The mass conservation equation for q phase is given by:

$$\frac{\partial}{\partial t}\left(\alpha_q \rho_q\right) + \nabla.\left(\alpha_q \rho_q \vec{v}_q\right) = \sum_{p=1}^{n} \dot{m}_{pq} \quad (1)$$

Where α is the phase volume fraction of phase q, ρ, the density, $\vec{v}$, the velocity vector, $\dot{m}_{pq}$ characterizes the mass transfer rate from phase q to phase p and n, the number of phases.

The momentum conservation equation for q phase is given by:

$$\frac{\partial}{\partial t}\left(\alpha_q \rho_q \vec{v}_q\right) + \nabla.\left(\alpha_q \rho_q \vec{v}_q \vec{v}_q\right) = -\alpha_q \nabla p + \nabla.\bar{\bar{\tau}}_q + \alpha_q \rho_q \vec{g}_q + \sum_{p=1}^{n}\left(\vec{R}_{pq} + \dot{m}_{pq}\vec{v}_{pq}\right) + \alpha_q \rho_q \left(\vec{F}_q + \vec{F}_{lift,q} + \vec{F}_{vm,q}\right) \quad (2)$$

Where $\bar{\bar{\tau}}$ s is the stress-strain tensor, $\vec{R}_{pq}$ an interaction force between phases, $\vec{F}_q$ is an external body force,, $\vec{F}_{lift,q}$ is a lift-force, $\vec{F}_{vm,q}$ is a virtual mass force, p is the pressure shared by all phases, and $\vec{g}$ is the gravitational acceleration vector.

The energy conservation equation for q phase is given by:

$$\frac{\partial}{\partial t}\left(\alpha_q \rho_q h_q\right) + \nabla.\left(\alpha_q \rho_q \vec{v}_q h_q\right) = -\alpha_q \frac{\partial p}{\partial t} + \bar{\bar{\tau}}_q : \nabla \vec{v}_q - \nabla.\vec{q}_q + S_q + \sum_{p=1}^{n}\left(Q_{pq} + \dot{m}_{pq} h_{pq}\right) \quad (3)$$

Where h is the specific enthalpy, $\vec{q}$ is the heat flux vector, S is the source term, Q is the intensity of heat exchange between the different phases, and h_{pq} is the difference in the formation enthalpies of phases p and q.

The heat exchange between phases must comply with the local balance conditions, as well as the interfacial mass, momentum interfacial exchange:

$$Q_{qp} = -Q_{pq}, Q_{qq} = 0 \quad (4)$$

$$\dot{m}_{pq} = -\dot{m}_{pq}, \dot{m}_{qq} = 0 \quad (5)$$

$$\vec{R}_{qp} = -\vec{R}_{pq}, \vec{R}_{qq} = 0 \quad (6)$$

B. Mass equation

The rate of vapor formation per unit volume in Eqs. 1 can be written as:

$$\dot{m}lv = \frac{h_{lv}\left(T_{lv} - T_s\right)A_l}{L} + \frac{\ddot{q}_E A_w}{L + C_{pl}\max\left(0, T_s - T_l\right)} \quad (7)$$

The first term is the mass exchange at the bubble surface and the second term represents the bubble formation due to heat flux at the wall. Here:

- $h_{lv} = \frac{\lambda_l}{d_v} Nu = \frac{\lambda_l}{d_v}\left(2 + 0.6 Re^{1/2} Pr^{1/3}\right)$ (8)

is the interfacial heat transfer coefficient calculated using the Ranz-Marshall correlation, where d_v is the diameter of the secondary phase (vapor bubble), λ_l is the liquid heat conductivity. Re, Pr and Nu are Reynolds number, Prandtl number and Nusselt number respectively:

- $A_i = 6\alpha_{sv}\left(1 - \alpha_v\right)/d_v$ (9)

is the interfacial area density, with α_v is the vapor volume fraction and $\alpha_{sv} = min(\alpha_v, 0.25)$ [22];

- $\ddot{q}_E$ = evaporating heat flux calculated from the RPI model [22, 23];
- $L = (h^0_{vs} - h^0_{ls})$ = latent heat per unit mass
- $A_w = \delta(\vec{x} - \vec{x}_w)$ = interfacial area density of the wall surface.

Subscripts l, v and s mean liquid phase, vapor phase and saturation state, respectively.

ISSN: 2356-5608

C. Momentum equation

The interfacial drag force between liquid and vapor phases per unit volume is calculated as:

$$\vec{R}_{lv} = 0.75 C_d \rho_l \alpha_v \vec{v}_r \left|\vec{v}_r\right| / d_v \quad (10)$$

where C_d is the drag coefficient determined by choosing the minimum of the viscous regime C_d^{vis} and the distorted regime C_d^{dis}:

$$C_d = Min\left(C_d^{vis}, C_d^{dis}\right) \quad (11)$$

The lift coefficient is calculated as (Moraga et al. [24]):

$$C_l = \begin{cases} 0.0767, \varphi \le 6000 \\ -\left[0.12 - 0.2\exp\left(-\frac{\varphi}{36000}\right)\right]\exp\left(\frac{\varphi}{3e7}\right), 6000 \le \varphi \le 190000 \\ -0.002, \varphi \ge 190000 \end{cases} \quad (12)$$

where $\varphi = Re_b Re_v$.

This lift coefficient combines the opposing action of two lift forces:

- Classical aerodynamic lift force resulting from the interaction between bubble and liquid shear,
- Lateral force resulting from the interaction between bubble and vortices shed by the bubble wake.

Here, $Re_b = \frac{d_v\left|\vec{v}_r\right|}{\nu_l}$ is the bubble Reynolds number and $Re_v = \frac{d_v^2\left|\nabla \times \vec{v}_l\right|}{\nu_l}$ is the bubble shear Reynolds number.

D. Turbulence model

The mixture turbulence model, default multiphase turbulence model, was used. It represents the first extension of the single-phase k-ε model. In the present case, using mixture properties and mixture velocities is sufficient to capture important features of the turbulent flow. The equations describing this model are respectively:

$$\frac{\partial}{\partial t}\left(\rho_m k\right) + \nabla.\left(\rho_m \vec{v}_m k\right) = \nabla.\left(\frac{\mu_{t,m}}{pr_k}\nabla k\right) + G_{k,m} - \rho_m \varepsilon + S_k \quad (13)$$

$$\frac{\partial}{\partial t}\left(\rho_m \varepsilon\right) + \nabla.\left(\rho_m \vec{v}_m \varepsilon\right) = \nabla.\left(\frac{\mu_{t,m}}{pr_\varepsilon}\nabla \varepsilon\right) + \frac{\varepsilon}{k}\left(C_{\varepsilon 1} G_{k,m} - C_{\varepsilon 2}\rho_m \varepsilon\right) + S_\varepsilon \quad (14)$$

where ρ_m and $\vec{v}_m$ are the mixture density and velocity, $\mu_{t,m}$ is the turbulent viscosity, $G_{k,m}$ is the production rate of turbulence kinetic energy, k is the turbulent kinetic energy, ε is the dissipation rate. $C_{\varepsilon 1}$ and $C_{\varepsilon 2}$ are constants.

This model contains two additional terms describing additional bubble stirring and dissipation. S_k is the bubble-induced turbulence in the turbulent kinetic energy equation and S_ε the bubble-induced dissipation in the dissipation rate equation:

$$S_k = \frac{0.75 C_d \rho_l \alpha_v \left|\vec{v}_r\right|^2}{d_v} \quad (15)$$

$$S_\varepsilon = S_{\varepsilon 3}\frac{3C_d\left|\vec{v}_r\right|}{d_v} S_k \quad (16)$$

with $C_{\varepsilon 3} = 0.45$

The turbulent diffusion force is calculated as [23]:

$$\vec{F}_v = -\vec{F}_l = -C_{TD}\rho_l k \nabla \alpha_v \quad (17)$$

with C_{TD} is the turbulent dispersion coefficient $C_{TD} = 1$. This force simulates liquid turbulence induced diffusion of bubbles from the wall into the liquid bulk.

E. Wall boiling model

According to the basic Rensselaer Polytechnic Institute (RPI) model [22], the total heat flux from the wall to nucleate boiling consists of three different components, namely the convective heat flux, the quenching heat flux, and the evaporative heat flux:

$$\dot{q}_W = \dot{q}_C + \dot{q}_Q + \dot{q}_E \quad (18)$$

The heated wall surface is subdivided into a portion Ω ($0 \le \Omega \le 1$) covered by nucleating bubbles and the rest of the surface area (1-Ω), is covered by the liquid.

- The convective heat flux is expressed as:

$$\dot{q}_C = h_c\left(1-\Omega\right)\left(T_w - T_l\right) \quad (19)$$

where h_C is the single phase heat transfer coefficient, and T_w and T_l are the wall and liquid temperatures, respectively.

- The quenching heat flux models the cyclic averaged transient energy transfer related to liquid filling the wall vicinity after bubble detachment, and is expressed as:

$$\dot{q}_Q = 2\Omega\left(\frac{f\lambda_l\rho_l C_{pl}}{\pi}\right)^{0.5}\left(T_w - T_l\right) \quad (20)$$

where f is the bubble departure frequency, λ, the thermal conductivity, C_p,the specific heat, and ρ, the density.

- The evaporative flux is given by :

$$\dot{q}_E = \frac{\pi}{6} d_{bw}^3 f \rho_v N_a L \quad (21)$$

Where d_{bw} is the bubble departure diameter, ρ_v, the vapor density, N_a, the active nucleate site density.

These equations need closure for wall boiling parameters:

1) Bubble Departure Diameter: The default bubble departure diameter (mm) for the RPI model is based on empirical correlations and is estimated as:

$$d_{bw} = Min\left(0.0014, 0.0006\exp\left(-\frac{T_{sub}}{45}\right)\right) \quad (22)$$

with $T_{sub} = T_{sat} - T_l$ the sub-cooling temperature.

2) *Nucleate Site Density:* The nucleate site density is represented by a correlation [24] based on the wall superheat $(T_w - T_{sat})$ as follow:

$$N_a = \left[200\left(T_w - T_{sub}\right)\right]^{1.8} \quad (23)$$

ISSN: 2356-5608

3) *Frequency of Bubble Departure:* The bubble departure frequency is calculated as:

$$f = \left[\frac{4g(\rho_l - \rho_v)}{3\rho_l d_{bw}}\right]^{0.5} \quad (24)$$

4) *Area density:*

The effective wall area occupied by boiling sites definition is based on the departure diameter and the nucleate site density:

$$\Omega = Min\left(1, N_a K\left(\frac{\pi d_{bw}^2}{4}\right)\right) \quad (25)$$

Where $K = 4.8exp(-Ja_{sub}/80)$, and $Ja_{sub} = \frac{(\rho_l C_{pl} T_{sub})}{\rho_v L}$ is the Jacob number [25].

5) *Bubble diameter*

The bubble diameter in the free stream is correlated with the local sub-cooling temperature $T_{sub} = T_{sat} - T_l$

$$d_v = \begin{cases} 1.5\times10^{-4}, T_{sub} > 13.5K \\ 1.5\times10^{-3} - 10^{-4}\times T_{sub}, 0 < T_{sub} < 13.5K \\ 1.5\times10^{-3}, T_{sub} < 0 \end{cases} \quad (26)$$

III. CFD Modelling

Mathematical model utilized in this paper was developed and then applied in CFD codes to be finally implemented in ANSYS-FLUENT via user-defined functions (UDFs) in conjunction with the Eulerian multiphase model in which the conservation equations are written for each phase, liquid and vapor [8,9].

The commercial CFD code ANSYS-FLUENT 12.0 [26] is used to perform the simulations. The interfacial forces models and the wall boiling model described previously were implemented in the code through User-Defined Functions (UDFs). The stainless-steel made vertical tube is 1m in length and 10 mm in diameter. Wall thickness is fixed to 2 mm. The sub-cooled water enters the system at the bottom, and then boils due to the constant heat flux supplied from the pipe walls.

A. Mesh geometry

The geometry used for problem formulation was two-dimensional axi-symmetric. Quadrilateral computational mesh is recommend for Eulerian multiphase model [27]. We started first to find the best computational meshes, Figure 1 shows the adopted grid consisting uniform rectangular cells.

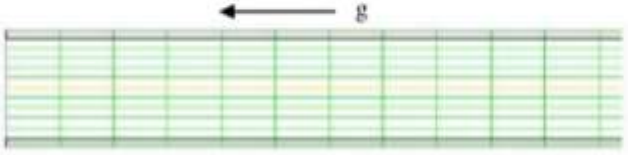

Fig. 1 Mesh geometry

B. Initial and Boundary conditions

Bubble pump saturation temperature is fixed to 425.15 K corresponding to the operating pressure of the machine. Fixed sub-cooling temperature (T_{sub} = 5K) and fully-developed profile of velocity are applied at the inlet (no vapor at the inlet α_{in}= 0). No-slip conditions on the tube wall. Liquid-vapor mixture leaves the tube at the saturation temperature. Heat Flux are specified at the external wall. The effect of the heat distribution is investigated for various heating rates ranging between 628 and 1728 W. At the interface wall-liquid, the UDFs was used to specify heat flux and heat transfer coefficient. Symmetry is used at the centreline axis.

C. Solution techniques

Unsteady state calculations with a time step of 0.1s were performed for all cases. SIMPLE algorithm was applied for the calculations of the pressure velocity-coupling with first order upwind calculation scheme for the discretization of momentum, energy and volume fraction equations.

IV. Numerical Model Validation

To examine the validity of the mathematical model, using ANSYS-FLUENT, the numerical predictions are compared [27, 28, 29] with the experimental data of Bartolomei and Chanturiya [30]. Braz Filho [27] proved that ANSYS-FLUENT code results are in reasonable agreement with the experimental data for void fraction and in excellent agreement for inner wall temperature evolution versus the fluid enthalpy, figure 2.

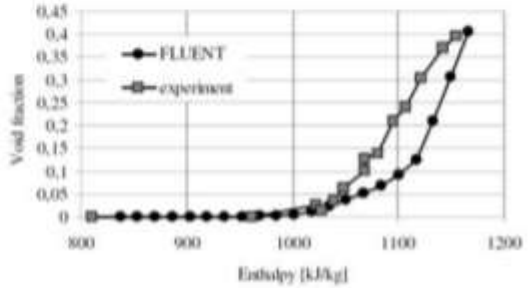

Model validation: Void fraction vs. Enthalpy

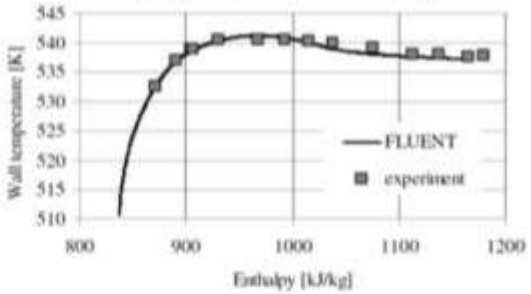

Model validation: Wall temperature vs. Enthalpy

Fig.2 Model validation :Void fraction and wall temperature vs. Enthalpy [27]

ISSN: 2356-5608

The predictions of axial distribution of average void fraction along the tube length [28] show an excellent agreement with experiments, figure 3.

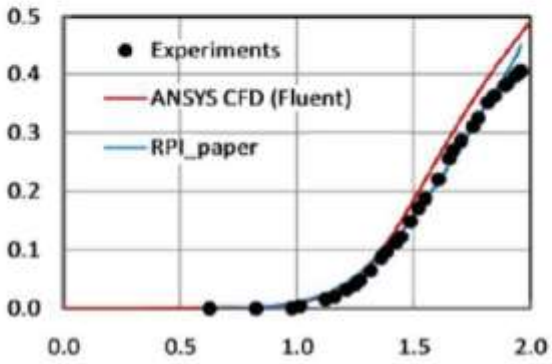

Fig.3 Model validation: Void fraction along tube length [28]

V. BUBBLE PUMP HEATING MODELS

For the purposes of the present study, two bubble pump models are treated - uniformly and partially heated tube as it is previously mentioned - to show the heat distribution effect on the boiling flow characterization. Heat flux is supplied to the bubble pump wall according to the following configurations:

- **Test 1**: Uniformly heated pump, full-length heating pipe, as depicted in Figure 4.
- **Test 2**: The heat flux is supplied in the lower 1/3 of the tube length (30 cm), partial-length heating pipe, as indicated in figure 5.

The boiling flow characteristics of bubble pump including void fraction evolution and flow pattern arrangement throughout the tube are investigated for various heat inputs from 628 (minimum heat flow rate for starting boiling) to 1728 W (beyond this limit: transition to annular flow not interesting for the bubble pump applications).

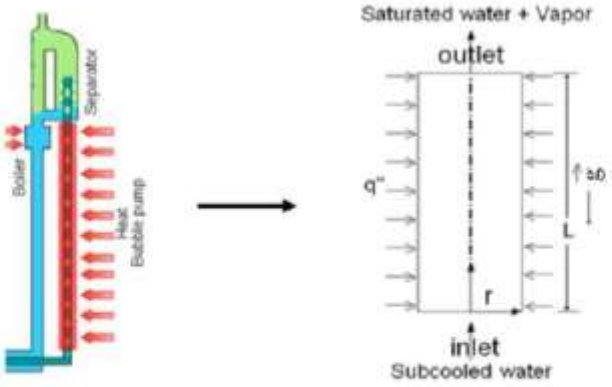

Fig. 4Test1: Uniformly heated bubble pump.

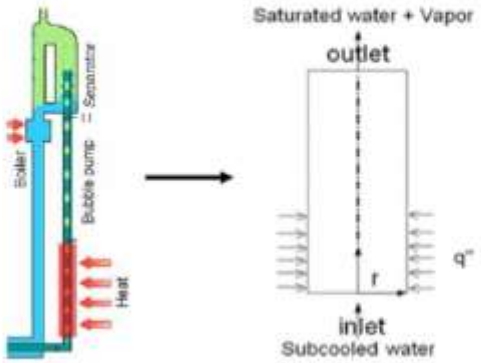

Fig. 5 Test2: Partially heated bubble pump

VI. RESULTS AND DISCUSSION

A. *Effect of heating configuration on void fraction profiles*

Figures 6 and 7 depict the effect of the heat inputs on the void fraction profiles along the bubble pump for various heat inputs from 628 to 1728 W respectively for test 1 (Uniformly heated tube) and test 2 (partially heated tube).

One can see in the two cases that the higher the heat is, the lower is the start up of boiling and the higher is the void fraction. In fact, when the heat input is increased from 628 W to 1728 W, the onset boiling length is reduced from 96 to 15 cm for uniformly heated pipe and from 5 to 1.5 cm for the partially heated one. Here, one can obviously remark how greatly this parameter is sensitive to the heating repartition. Actually, for the same heat input, 628 W, boiling starts at 96 cm in the first heating model (test1) and at 15 cm in the second one (test2) which can be explained by the higher heat density in the bottom of the tube; which have a great impact on the performances of the bubble pump, flow regime repartition, liquid vapour velocities arrangement and temperature profiles [31, 32].

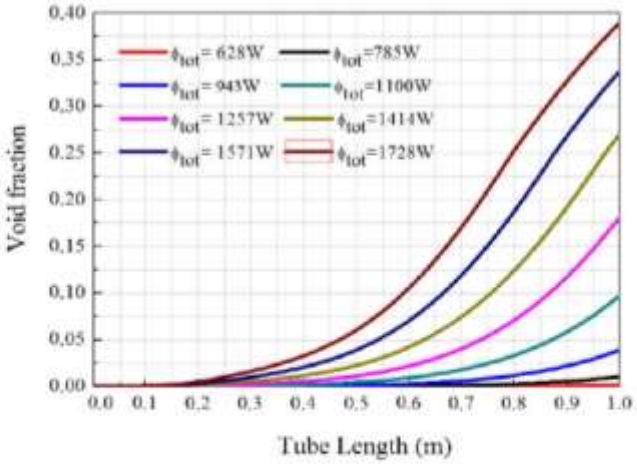

Fig. 6Void fraction evolution of the uniformly heated pump (test1) for different heat fluxes

ISSN: 2356-5608

On the other hand, the void fraction at the tube outlet is increased from 0.001 to 0.39 and from 0.22 to 0.58 respectively for the totally heated tube and the partially heated tube. One also can observe, as illustrated in figure 8, that for the first heating model the void fraction increases slightly over the whole tube length [8, 9], attains a value of 0.016 at z = 30 cm and a maximum of 0.39 at the tube outlet for Φ_{tot} = 1728 W.

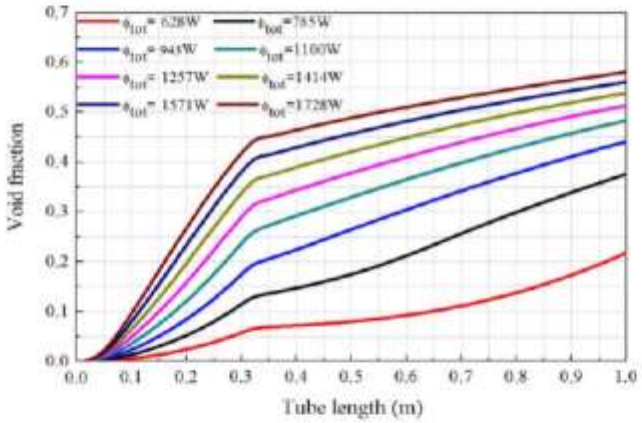

Fig. 7Void fraction evolution of the partially heated pump (test2) for different heat fluxes

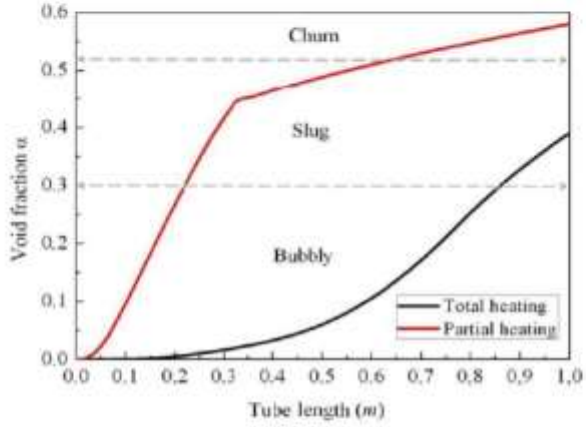

Fig. 8Void fraction distribution for Φ=1728W

This behavior is completely different from that of the second heating model. In fact, for this case (test 2) the void fraction rises sharply, reaches a value in the order of 0.42 at the outlet of the heated zone (z =30 cm) and then increases slightly over the remaining length of the tube to attain a maximum of 0.58 at the outlet. The same remark can be observed for the other heat inputs as shown in figure 9.

B. Identification of different flow regimes in the bubble pump

In this section the void fraction is used to predict the flow regime repartition in the thermally driven bubble pumps. As it was previously reported, the critical void fraction for bubbly-to-slug, slug-to-churn and churn-to-annular transition are respectively 0.3, 0.52, and 0.8. Figures 9 and 10 show the flow patterns limit for different heating distribution and heat fluxes. Specially, the heating repartition effect can be remarked.

Tables I recapitulate the length of the zone occupied by different flow regimes along the bubble pump for each heating configuration and various tested heating power.
One can remark that as we reduce the heating power, the slug zone length is reduced to disappear completely at low heat input for partially heated tube (test2). In fact, it is reduced from 69 cm to 20 cm when the heat input reduced from 1257 to 785W before totally disappearing for 628W. Nevertheless, the bubbly flow regime occupies the hall tube length for all previous heat input ranging from 785 to 1257W when the pump is uniformly heated (test1).

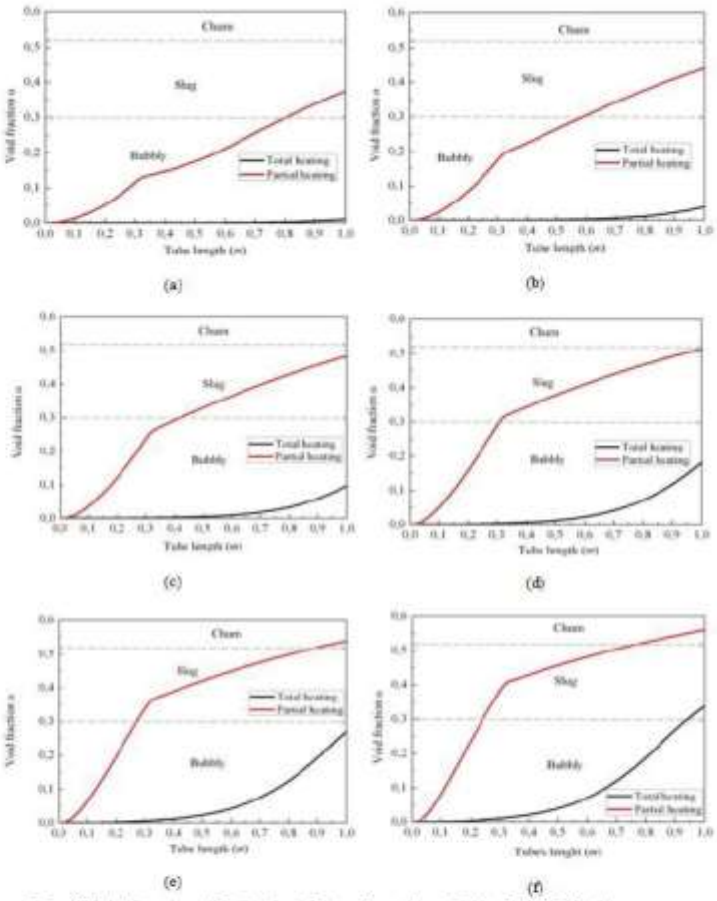

Fig. 9Void fraction distribution for test1 and test 2 (a): Φ=785W, (b): Φ=943W, (c): Φ=1100W, (d): Φ=1257W, (e): Φ=1414W, (f): Φ=1571W

The same table show that increasing heat input from 1414W to 1728W decreases the slug zone length from 63cm to 43cm in favour of the churn flow zone which increases from 10 to 35cm in case of the partial heating configuration. As regards the uniformly heated configuration, the slug flow

ISSN: 2356-5608

zone length varies from 0 to 14 cm to occupy part the bubbly flow zone for the same variation of heat input to the bubble pump, namely from 1414 to 1728W.

VII. Conclusion

Numerical simulation of the heating distribution effect on the boiling flow of water in vertical tube was carried out with the commercial CFD package ANSYS-FLUENT. User defined Functions (UDFs) are employed to model the boiling phenomena. Void fraction distributions are calculated, discussed and then flow patterns throughout the tube length are predicted. It was found that the void fraction is higher when heating partially the wall. Flow regimes repartitions are identified referring to the void fraction variation along the tube. It was found that the void fraction at the tube outlet is higher for the partially heated tube then the totally heated tube. Moreover, when the heating power, is increased for the partially heated tube, the slug flow zone length first increases and then decreases in favour of the churn flow regime.

TABLE I
ZONE REGIME LENGTH FOR FULL AND PARTIAL LENGTH HEATED TUBEAT VARIOUS HEAT INPUT

Heating at **628W**	Zone regime length (m)		
	Bubbly	Slug	Churn
Test 1	**1**	**0**	**0**
Test 2	**1**	**0**	**0**
Heating at **785W**	Zone regime length (m)		
	Bubbly	Slug	Churn
Test 1	**1**	**0**	**0**
Test 2	**0.80**	**0.20**	**0**
Heating at **943W**	Zone regime length (m)		
	Bubbly	Slug	Churn
Test 1	**1**	**0**	**0**
Test 2	**0.59**	**0.41**	**0**
Heating at **1100W**	Zone regime length (m)		
	Bubbly	Slug	Churn
Test 1	**1**	**0**	**0**
Test 2	**0.42**	**0.58**	**0**
Heating at**1257W**	Zone regime length (m)		
	Bubbly	Slug	Churn
Test 1	**1**	**0**	**0**
Test 2	**0.31**	**0.69**	**0**
Heating at **1414W**	Zone regime length (m)		
	Bubbly	Slug	Churn
Test 1	**1**	**0**	**0**
Test 2	**0.27**	**0.63**	**0.1**
Heating at **1571W**	Zone regime length (m)		
	Bubbly	Slug	Churn
Test 1	**0.94**	**0.06**	**0**
Test 2	**0.244**	**0.536**	**0.22**
Heating at **1728W**	Zone regime length (m)		
	Bubbly	Slug	Churn
Test 1	**0.86**	**0.14**	**0**
Test 2	**0.22**	**0.43**	**0.35**

VIII. References

[1] B.C. Von Platen, C.G. Munters, US Patent 1, 685,764, 1928.

[2] A. Zohar, M. Jelinek, A. Levy, I. Borde, The influence of the generator and bubble pump configuration on the performance of diffusion absorption refrigeration (DAR) system, International journal of refrigeration, 31 (2008) 962–969.

[3] B. Pasupathy, A. Mani, Numerical Studies on Vertical Tubular Generator in Vapour Absorption Refrigeration System, International Refrigeration and Air Conditioning Conference at Purdue, July 12-15, 2010.

[4] Zh. Ma, A. Turan, and Sh. Guo, Practical Numerical Simulations of Two-Phase Flow and Heat Transfer Phenomena in a Thermosyphon for Design and Development, ICCS, Part I, LNCS 5544, (2009) 665–674, Springer-Verlag Berlin Heidelberg.

[5] Ahmed Taieb, Khalifa Mejbri, Ahmed Bellagi, Theoretical analysis of a diffusion-absorption refrigerator, International journal o f hydrogen energy 41 (2016) 14293-14301.

[6] Ahmed Taieb, Khalifa Mejbri, Ahmed Bellagi, Detailed thermodynamic analysis of a diffusion-absorption refrigeration cycle, Energy 115 (2016) 418-434.

[7] Almen GC. Gas absorption Refrigerator technology. ABS reftec; 2003. http://www.absreftec.com/index.html [accessed 13.09.12].

[8] R. Garma, Y. Stiriba, M. Bourouis, and A. Bellagi, Numerical Investigation of Nucleate Boiling Flow in Vertical Tubes, 2nd International Symposium on Energy CIE'12, March 26-28 (2012) Tozeur, Tunisia. Comm039.

[9] R. Garma , M. Bourouis , A. Bellagi, Numerical Investigation of Nucleate Boiling Flow in Water Based Bubble Bumps International Journal of Fluid Mechanics & Thermal Sciences; 1(2015): 36-41.

[10] N. Ben Ezzine, R. Garma, M. Bourouis, A. Bellagi, Experimental Studies on Bubble Pump Operated Diffusion Absorption Machine Based on Light Hydrocarbons for Solar Cooling, Renewable Energy, 35 (2010) 464-470.

[11] S. Mazouz, N. Ben Ezzine, R. Garma, M. Bourouis, A. Bellagi, Experimental Investigation and Theoretical Model of a Diffusion Solar Absorption Machine, International Sorption Heat Pump Conference, September 23-26 (2008) Seoul, Korea, Comm AB-072.

[12] U. Jacob, and U. Eicke, Solar cooling with diffusion absorption principal, Proceeding of the 7th World Renewable Energy Congress, WREN, U.K., (2002)1-5

[13] U. Jacob, U. Eicker, D. Schneider, A.H. Taki, and M.J. Cook, Development of an optimized solar driving diffusion-absorption cooling machine, Proceeding of the ISES Solar Xorld Congress, June 16-19, ISES, Goteborg (2003) 1-6.

[14] U. Jacob, U. Eicker, D. Schneider, A.H. Taki, and M.J. Cook, Development of a solar powered diffusion absorption cooling machine, Proceeding of the 1st International Conference Solar Air-Conditioning, October 6-7, Staffelstein, Germany (2005) 111-115.

[15] U. Jacob, U. Eicker, D. Schneider, A.H. Taki, and M.J. Cook, Simulation and experimental investigation into diffusion absorption cooling machines for air-conditioning application, Applied Thermal Engineering, 28 (2008) 1138–1150.

[16] N. A. Radovicich and R. Moissis, The transition from two-phase bubble flow to slug flow, MIT Report No. 7 (1962) 7633-22.

[17] Y. Taitel, D. Bornea, and A. E. Dukler, Modelling flow pattern transitions for steady upward gas-liquid flow in vertical tubes, AIChE J. 26 (1980) 345-354.

[18] K. Mishima, and M. Ishii, Flow regime transition criteria for upward two-phase flow invertical tubes, Int. J. Heat and Mass Transfer 27 (1984) 723-737.

[19] N. Brauner, and D. Barnea, Slug/churn transition in upward vertical flow, Chem. Eng. Sci. 41 (1986) 159-163.

[20] D. Barnea, A unified model for predicting flow-pattern transitions for the whole range of pipe inclinations, Int. J. Multiphase Flow 13 (1987) 1-12.

[21] G. B. Wallis, One-Dimensional Two-Phase Flow, (1969) McGraw-Hill, New York

[22] R.M. Podowski, D.A. Drew, R.T.J. Lahey, M.Z. Podowski, A mechanistic model of the ebullition cycle in forced convection subcooled boiling, Eighth International Topical Meeting on Nuclear Reactor Thermal Hydraulics, Kyoto, Japan, 3(1997)1535-1542.

[23] N. Kurul, M.Z. Podowski, Multidimensional effects in forced convection subcooled boiling, Ninth International Heat Transfer Conference, Jerusalem, Israel, August 19-24 (1990) 21-26.

ISSN: 2356-5608

[24] F.J. Moraga, F.J. Bonetto, R.T. Lahey, Lateral forces on spheres in turbulent uniform shear flow, Int. J.Multiphase Flow, 25(1999)1321-1372.
[25] D.B.R. Kenning, H.T. Victor, Fully-developed nucleate boiling: Overlap of areas of influence and interference between bubble sites, Int. J. Heat Mass Transfer 2 (1981)1025-1032.
[26] ANSYS FLUENT Theory Guide. Release 12.0. ANSYS, Inc. April 2009.
[27] F.A. Braz Filho, A.D. Caldeira and E.M. Borges, Validation of a multidimensional computational fluid dynamics model for subcooled flow boiling analysis, International Nuclear Atlantic Conference - INAC 2011 Belo Horizonte, MG, Brazil, October 24-28 (2011) ASSOCIAÇÃO BRASILEIRA DE ENERGIA NUCLEAR - ABEN.
[28] G. Eggenspieler, Multiphase Models in ANSYS CFD, 2011 ANSYS, Inc. May 14 2012.
[29] Fluent Tutorial: Modeling Nucleate Boiling Using FLUENT.
[30] G. G. Bartolomei and V. M. Chanturiya, Experimental Study of True Void Fraction When Boiling Subcooled Water in Vertical Tubes, Thermal Engineering 14 (1967) 123-128.
[31] R. Garma, Y. Stiriba, M. Bourouis, A. Bellagi, Numerical Investigations of the Heating Distribution Effect on the Boiling Flow in the Bubble Pumps, International Journal Of Hydrogen Energy, 39 (2014) 15256–15260.
[32] R. Garma, Youssef stiriba, M. Bourouis, and A. Bellagi. 2012. Numerical Investigation of Nucleate Boiling Flow in Vertical Tubes, 2nd International Colloque of Energy, CIE'12, March 26-28 (2012)

ISSN: 2356-5608